OVERVIEW OF PLASMA EDGE PHYSICS

Bernhard Unterberg
Institut für Plasmaphysik, Forschungszentrum Jülich GmbH*, Association EURATOM-FZ Jülich
D-52425 Jülich, Germany, phone: +49 2461 61 4803, email: B.Unterberg@fz-juelich.de

ABSTRACT

Basic properties of the plasma edge in magnetically confined fusion plasmas are summarized. Starting from the magnetic topology of tokamaks we describe the transport of the scrape-off layer including drifts, the transition to high recycling and detached plasma regimes typical for divertors and the consequences of the electrostatic Debye sheath in front of the plasma facing components. The transport of the fuel neutrals (hydrogen atoms and molecules) is described and the concept of power exhaust from line radiation of impurities at the plasma edge is introduced.

I. INTRODUCTION

Processes at the edge plasma in general and plasma-wall interaction in particular play a crucial role for achieving a steady state burning fusion plasma. The first wall has to withstand and exhaust the α- particle heating power and the helium-ash must be removed (pumped) from the plasma. Wall erosion affects the lifetime of wall elements and releases impurities into the plasma, which then cause fuel dilution and energy loss due to radiation from the plasma centre. Moreover, also global confinement properties can be affected by edge processes. Therefore, understanding these processes and controlling the edge plasma by appropriate means is an important field of research.

The plasma in a tokamak or stellarator represents an open system. The wall is a perfect plasma sink and owing to the finite confinement times (energy and particle confinement times τ_E and τ_P) the plasma has to be renewed continuously. The energy content E is sustained by heating, $E = P_{heat} * \tau_E$, with the heating power P_{heat}. The number N of particles in the plasma is sustained by a permanent flow of D/T gas from the wall elements into the plasma, $N = \Gamma * \tau_p$. The alpha particles with a power density of $P_\alpha = 0.15 MW/m^3$ (T=10 keV, $n = 10^{20} m^{-3}$) lead to an average wall load of some $100 kW/m^2$, if we take into account a plasma volume of roughly $1000 m^3$ for self- sustained burn - a moderate value. However, energy exhaust becomes a problem, because the magnetic field directs the convected heat load on rather small wall areas. This can lead to peak loads which could damage the wall.

Another important issue of edge physics is impurity generation and impurity exhaust. Any impurities in the plasma centre lead to fuel dilution reducing the fusion power. Their concentration has to stay below a certain level. E.g. the concentration of the unavoidable helium, which is generated at a rate of $R_{He} = 10^{18} s^{-1} m^{-3}$, should not exceed significantly a value of about 10%. This condition is fulfilled when the characteristic time $\tau^*_{p,He}$ for helium removal is sufficiently low [8], [9]. The experimental values found for $\tau^*_{p,He}$ are much larger (factor 10 or more) than the global confinement time of helium demonstrating that helium is recycling at the wall more than 10 times before it is removed by the pumps. The presence of other impurities in the plasma depends on the choice of wall materials, erosion processes and edge plasma properties, like temperature, density and particle transport.

No unique definition exists for the term "plasma edge" or "plasma boundary". An important part of the edge plasma is the scrape-off layer (SOL) which is that region of the plasma where the magnetic field lines intersect wall elements. But significant processes occur also inside the confined plasma, like neutral particle penetration, ionization, charge exchange or impurity line radiation. These atomic processes have an impact on the properties of both, the edge plasma and the core plasma.

In this lecture plasma edge physics is introduced comprising the SOL as well as part of the confined plasma. The relevant processes are discussed following the transport cycle of the particles beginning with the boundary conditions which are given by the magnetic topology. After an illustration of the basic SOL properties, we discuss the penetration of neutrals into the plasma. Then a general description of the parallel transport in the SOL is given. Next, we introduce the Debye sheath in front of the plasma facing components, before we discuss the properties of the simple

*Partner in the Trilateral Euregio Cluster

limiter SOL and the complex divertor SOL. Finally, we close with a section on impurity transport and radiation, where we discuss both the SOL and the confined plasma. Here, the cold and radiating plasma mantle is introduced as a possible concept for power exhaust from fusion plasmas. Overall, the physical processes in the plasma edge have important consequences for the interaction between plasma and wall and the resulting recycling and erosion mechanisms. This subject is discussed in a separate lecture [1].

An excellent introduction into the physics of the plasma boundary can be found in the book of P.C. Stangeby "The Plasma Boundary of Magnetic Fusion Devices" [2]. Further monographs used for this overview have been published by A.V. Nedospasov and M.Z. Tokar [3] and R. Schneider [4], a review article on experimental divertor physics by C.S. Pitcher and P.C. Stangeby is published in [5].

II. MAGNETIC TOPOLOGY

Wall elements which intersect the magnetic field serve as a perfect plasma sink and impose a flow directed along the field lines. The flux tubes generated at each wall element are filled with plasma by perpendicular transport (diffusion, drifts). This property helps to build up a particle density sufficient for helium exhaust. On the other hand the concentration of plasma flow on small areas is less beneficial for power exhaust, since a uniform plasma flow to the whole wall would avoid peak heat loads. The very details of particle and heat load on the wall are determined by the magnetic topology and the geometry of the plasma facing components. We have to distinguish two different concepts: divertor and limiter. The poloidal divertor shown in Fig. 1 is used in the performance oriented tokamak devices (JET, JT60-U, DIII-D, ASDEX-U) and is the preferred concept for the next step device. The simpler (and cheaper) limiter is explored e.g. in Tore Supra and TEXTOR (toroidal belt limiter), in particular, with respect to steady state technology, plasma-wall interaction and new concepts with ergodic boundaries. The subject of ergodic divertor physics is discussed in [6], for a review on divertor physics in stellarators the reader is referred to [7].

The projection of the flux tubes on the surface of the limiter/divertor plate is determined by two angles: the tilting angle α between toroidal and poloidal direction depends on the rotational transform (safety factor) q; the angle Ψ in the poloidal plane between the magnetic field and the surface normal is given by the limiter shape or the orientation of the divertor plates. In torus geometry α varies along the poloidal coordinate depending on the aspect ratio and the plasma pressure.

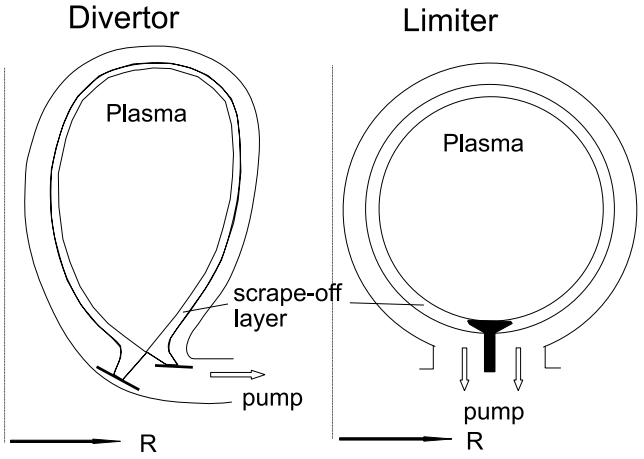

Figure 1: Poloidal divertor and toroidal limiter concept shown in the poloidal plane of a tokamak

III. BASIC CHARACTERISTICS OF THE SOL

Both concepts shown in fig. 1 are toroidally symmetric. This allows to discuss the main features by reducing the transport inside the SOL to a 2-dimensional problem: flow along the field line (coordinate z) and diffusion in radial direction (coordinate x) as shown in fig. 2. As we will see below, the radial extension of the SOL is small with respect to the minor radius of the plasma ($\lambda \ll a$), so that we can apply a plane geometry and straighten out the SOL as indicated in fig. 2, thereby neglecting toroidal effects.

The SOL begins at the last closed flux surface (LCFS). After the initiation of the plasma discharge and on a time scale of μs, electrons will rush ahead the ions as a consequence of their higher mobility and charge up the solid negatively. A thin sheath will form to shield the electrostatic potential with a characteristic length given by the so called Debye length

$$\lambda_D = \sqrt{\frac{\epsilon_0 k T_e}{n_e e^2}} \qquad (1)$$

For $T_e = 20eV$ and $n_e = 10^{19} m^{-3}$ we get $\lambda_D = 10^{-5} m$, which reflects the fact that the plasma maintains quasi- neutrality very well. Further properties of this sheath will be discussed in section VI.

However, the shielding is imperfect because of the thermal motion of the plasma particles and a small electric field penetrates the plasma (pre-sheath) which accelerates the ions towards the target. The electrons feel a corresponding retarding field. The plasma fluid as a whole is quasi- neutral, because of the plasma sink at the end of the field lines a pressure gradient develops and a symmetric flow towards both ends is driven. At the symmetry plane the parallel flow velocity $v_{\|}$ and the

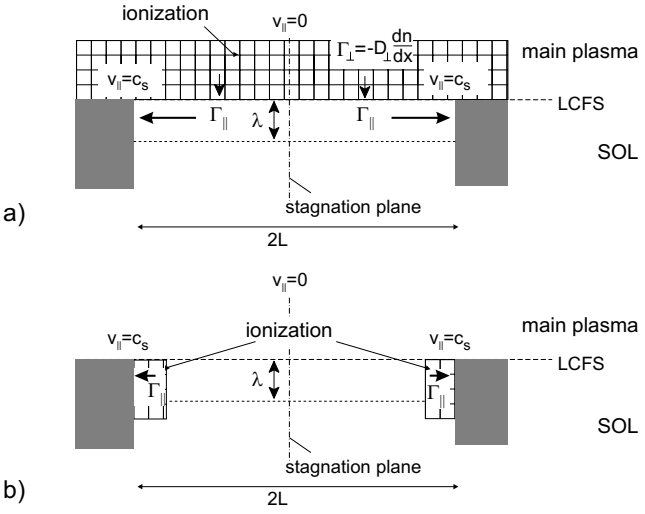

Figure 2: 2-d model of the SOL, a) simple SOL, b) complex SOL

parallel flux density $\Gamma_\parallel$ must be zero (stagnation plane) and at both ends the flow velocity reaches sound speed, $v_\parallel = c_s$ (so called the "Bohm criterion").

At the material surfaces ions and electrons recombine and are released back into the plasma as neutrals, will be ionized by impact of electrons and form the plasma source to drive again plasma flow back to the material surfaces. This process which has a very short time scale compared to the duration of a plasma discharge (e.g. in TEXTOR several tens of ms compared to 10 s) is called *recycling*. The recycling process is strongly influenced by the fact how the neutrals are released into the plasma and where they get ionized. Some characteristics of the transport of neutrals in the plasma edge are summarized in section IV. Much more details, in particular on techniques how to prescribe the neutrals in realistic geometry are given in [8]. Two different situations can be distinguished with respect to the particle sources in the SOL. Under the simplified assumption that there are no ionization sources in the volume of the SOL but the sources are located inside the confined volume, the SOL is solely filled by a cross-field diffusion with a flux density $\Gamma = -D_\perp \partial n/\partial x$. This situation is generally named the "simple SOL", cf. fig. 2a). On the other hand, if all ionization sources are located inside the SOL, no perpendicular diffusion into the SOL develops, cf. fig. 2b). While the first situation is usually realized in limiter tokamaks and in divertor tokamaks with low plasma densities, the second situation can only be realized in divertor tokamaks at high plasma densities and is usually called the "complex SOL" for reasons which will become clear in the following.

Throughout this overview we will describe the edge plasma in the fluid picture with equations for the average quantities rather than with a full kinetic analysis. Strictly, the requirement for such a procedure is that the self- collisional mean free pathes of electrons and ions $\lambda_{ee} \approx \lambda_{ii} \approx 10^{16} T^2/n$ (with T in eV and n in m^{-3} yielding $\lambda_{ee,ii}$ in m) are smaller than the extension of the plasma along the magnetic field (connection length L). In the medium size limiter tokamak TEXTOR with typical SOL parameters $L \approx 20m$, $n = 1 - 10 \cdot 10^{18} m^{-3}$ and $T = 10 - 100eV$ the mean free path is 0.1m (high density/ low temperature case) up to 100m (low density/ high temperature case) the situation can be marginal at SOL low densities.

With simple estimates we may now characterize some basic features of such a SOL as the SOL thickness and the radial density variation, assuming a simple SOL with perpendicular diffusion as particle source for the SOL. For this first estimate we may relate the length of the flux tube (connection length $2L$, where $L = \pi q_a R$ in a toroidal limiter / poloidal divertor configuration with q_a the safety factor at the edge and R the major radius) and the SOL thickness λ to the average transport velocities $v_\parallel$ and $v_\perp$ according to

$$\frac{v_\perp}{v_\parallel} = \frac{\lambda}{L}. \tag{2}$$

For the average velocities we take $v_\parallel = 0.5 c_s$ and $v_\perp n = D_\perp \partial n/\partial x$. With the characteristic length $\lambda = (1/n)\partial n/\partial x$ we obtain for Eq. 2

$$\frac{D_\perp/\lambda}{0.5 c_s} = \frac{\lambda}{L}. \tag{3}$$

From this relation we get the well known expression for the SOL thickness λ (i.e. the density decay length)

$$\lambda = \sqrt{\frac{D_\perp L}{0.5 c_s}} \tag{4}$$

With typical values for an edge plasma $D_\perp = 1m^2/s$, $T = 50eV$, and L=10 m we obtain $\lambda = 30mm$. This is a remarkably small value compared to the dimensions of a fusion reactor. As a consequence, the surface area wetted by the plasma reduces by roughly two orders of magnitude with respect to the total wall area, leading to unacceptable high heat loads. We will see later that this simple calculation even overestimates the SOL thickness, in particular close to the plasma facing components.

The radial variation $f(x)$ of density inside the SOL can be derived from a simple 1d-calculation based on the conservation of mass along the flow channel z

$$\frac{\partial}{\partial x} D_\perp \frac{\partial n}{\partial x} = \frac{\partial}{\partial z}(n v_\parallel). \tag{5}$$

Assuming in a first step $D_\perp = const$ and $\partial n/\partial x = const.$ along z as well as a constant r.h.s of Eq. 5 represented by $\partial/\partial z(nv_\parallel) = n/\tau_\parallel$ with a characteristic particle residence time in the SOL given by $\tau_\parallel$ (parallel transport to the target is the only plasma sink, no particle sources caused by ionization of neutrals inside the SOL are considered) we obtain the solution of Eq. 5

$$n(x) = n(0)\exp(-x/\sqrt{D_\perp \tau_\parallel}) \qquad (6)$$

The density shows an exponential decay inside the SOL with a characteristic length $\lambda = \sqrt{D_\perp \tau_\parallel}$ as given by Eq. 4, $n(0)$ denotes the density at the LCFS. Here, the typical time scale of parallel transport to the targets $\tau_\parallel$ is of the order of ms. However, one has to be careful when using these simple expressions, as particle sources inside the SOL and drifts will alter the result as discussed later on.

IV. NEUTRAL PARTICLE TRANSPORT

Hydrogen (deuterium or tritium) and impurity neutrals are released from the plasma facing components and penetrate into the edge plasma. Owing to the different release mechanisms as discussed in [1] we observe also different particle velocities. This has an important impact on the edge plasma.

Hydrogen may be released as a molecule H_2 or an atom H_0. It has been found that in the recycling process the probability for molecule formation depends on the surface temperature, which determines the residence time in the surface. At low temperatures mainly molecules are desorbed while above about $T_s = 1200K$ the majority of particles is released as atoms [17] [18].

Some processes involved with the penetration of H_2 are illustrated in Fig. 3 . Because of electron impact the molecule dissociates. Various dissociation channels compete, with cross sections depending on T_e. Some of them are given in table 1 together with the rate coefficients for T_e =50 eV.

The reaction no.1, also illustrated in Fig. 3, is only dominant at or below $T_e = 10eV$, whereas at higher T_e the molecule is first ionized and then dissociated (reactions no.3 and no.4), as is obvious from the rate coefficients $< \sigma v >_{dis}$ [19]. The atoms resulting from the dissociation of molecules in ground state gain energies in the range of $2.2eV$. Surprisingly, average energies significantly lower than these ($0.5eV$) have been measured in the vicinity of a limiter [20] [21]. It is assumed that this is caused by vibrationally excited molecules.

The probability that an atom has at least one charge exchange (CX) reaction before it is ionized is rather high because the rate coefficients for ionization

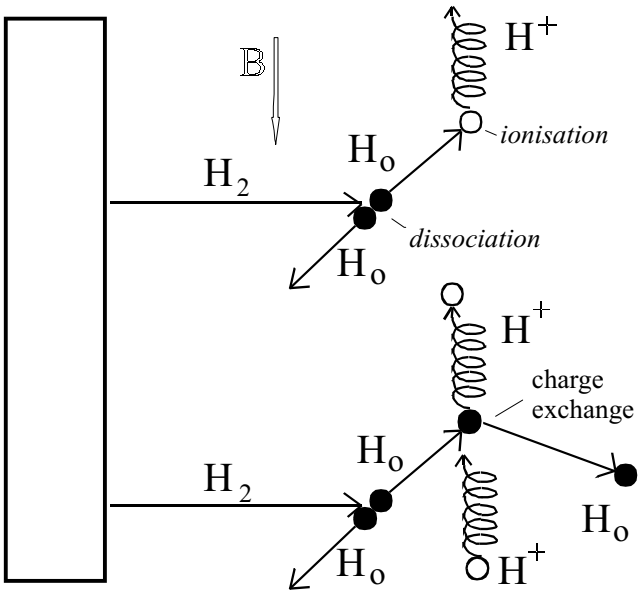

Figure 3: Molecule dissociation and charge exchange processes at the plasma boundary (solid circles: atoms, open circles: ions)

no.	dissociation reaction	$< \sigma v >_{dis} /m^3/s$
1	$H_2 \rightarrow H_0 + H_0$	$6 \cdot 10^{-15}$
2	$H_2 \rightarrow H_0 + H^+$	$2 \cdot 10^{-15}$
3	$H_2 \rightarrow H_2^+$	$4 \cdot 10^{-14}$
4	$H_2^+ \rightarrow H_0 + H^+$	$3 \cdot 10^{-13}$
5	$H_2^+ \rightarrow H^+ + H^+$	$6 \cdot 10^{-15}$

Table 1: Dissociation reactions of hydrogen molecules and molecular ions[19].

$< \sigma v >_i$ and CX $< \sigma v >_{CX}$ are similar as is shown in the table 2 [19].

Using the atomic and molecular data the transport of neutral particles can be modelled with a rather high accuracy even for complicated 3d-geometries [22] [8].

The velocity of *impurity* atoms also depends on their release mechanisms. The fastest particles are reflected impurities (impurity ions from the plasma, neutralized and re-emitted). Among the erosion mechanisms, sputtering generates particles in the range of 5 eV. Atoms coming from molecules gain their velocity from the dissociation energy. Sublimated or evap-

$T_e = T_i$	10	100	eV
$< \sigma v >_i$	$7 \cdot 10^{-15}$	$3 \cdot 10^{-14}$	$m^3 s^{-1}$
$< \sigma v >_{CX}$	$2 \cdot 10^{-14}$	$5 \cdot 10^{-14}$	$m^3 s^{-1}$

Table 2: Rate coefficients for ionization and charge exchange [19].

orated atoms have only thermal energy, thus represent the slowest particles with the least impact on the edge plasma (cf. discussion in [1]).

Recombination processes are generally not important unless the plasma is very cold as in detached divertors, since in most cases the recombination times of ions are much longer than the average residence time of the particles in the plasma.

The ionization time of an atom can be calculated from the rate coefficient for ionization $< \sigma v >_i (T_e)$ and the local electron density n_e. The time derivative of the neutral density n_0 owing to ionization is then given by

$$\frac{\partial n_0}{\partial t} = -n_e n_0 < \sigma v >_i \quad (7)$$

leading to an exponential decay of the atom density

$$n_0(t) = n_0(t=0)\exp(-\frac{t}{\tau_i}). \quad (8)$$

The ionization time τ_i is given by

$$\tau_i = \frac{1}{n_e < \sigma v >_i} \quad (9)$$

The penetration of neutral particles into a homogeneous plasma having a velocity v_0 is given by the ionization length

$$\lambda_i = \frac{v_0}{n_e < \sigma v >_i} \quad (10)$$

In the presence of a radial profile of both the electron density and temperature the description of the ionization length can be generalized to

$$\int_0^{\lambda_i} \frac{n_e(r) < \sigma v >_i (T_e(r))}{v_0} dr = 1 \quad (11)$$

We can define the ion source distribution $Q(r)$, which is given under steady- state conditions as

$$Q(r) = -\frac{\partial \Gamma_0}{\partial r} = n_0(r) n_e(r) < \sigma v >_i (T_e(r)) \quad (12)$$

Here, $\Gamma_0 = n_0 v_0$ is the neutral flux density under the simplifying assumption of a mono-energetic neutral velocity distribution. The ioniszation length λ_i can be used to characterize the radial extent of the ion source distribution. As a consequence the impact of neutrals on the edge plasma is characterized both by their velocities as determined by the specific release mechanism and the edge plasma parameters n_e and T_e.

As stated before, for hydrogen atoms charge exchange processes are important in addition. This gives rise to a diffusion process of the atoms. The penetration depth is given by the geometric mean of the ionization length λ_i as given by Eq. 10 and the mean free path for the CX process λ_{CX} [23] using for both (!) the thermal ion velocity $v_{th} = \sqrt{kT_i/m_i}$

$$\lambda_{pen} = \frac{v_{th}}{n_e \sqrt{< \sigma v >_{CX} < \sigma v >_i}}. \quad (13)$$

V. GENERAL DESCRIPTION OF PARALLEL TRANSPORT IN THE SOL

We start our general description of SOL transport parallel to the magnetic field (z direction) in the fluid picture with the conservation equations for particles, momentum and energy under steady- stated conditions (no partial time derivatives). The extension to 2D transport (parallel - radial) can be made by including "effective" cross field sources (cf. [2], chapter 13, and [3], section 1.1). We consider two species (electrons e and singly charged plasma ions i) under the assumption of quasi- neutrality ($n_e = n_i = n$).

$$\frac{\partial}{\partial z}(n_{i,e} v_{\parallel i,e}) = S_p \quad (14)$$

Here n denotes the particle density, $v_\parallel$ the parallel fluid velocity and S_p the particle source which can be related to particle transport into the SOL, to ionization or recombination processes (the latter forming a particle sink in the SOL volume).

Next we introduce the momentum equations for plasma ions of mass m_i in its conservative form

$$\frac{\partial}{\partial z}(m_i n v_{i,\parallel}^2 + p_i) = enE + R_{ie} + R_n. \quad (15)$$

Here $p_i = kT_i n$ is the ion pressure with T_i the ion temperature, k the Boltzmann constant, e the elementary charge, E the parallel electric field, R_{ie} the friction force term owing to collisions with electrons and R_n the friction force term owing to collisions with neutrals. Both friction terms have two contributions,

$$R_{ie} = m_e(v_e - v_i)\nu_{ei} n + 0.71 n \frac{\partial k T_e}{\partial z} \quad (16)$$

with m_e the electron mass, ν_{ei} the electron ion collision frequency and T_e the electron temperature, and

$$R_n = -m_i(v_i - v_n) < \sigma v >_{CX} n_n n + m_i v_n S_p \quad (17)$$

with v_n the velocity which with the neutrals with a Maxwellian distribution are drifting, $< \sigma v >_{CX}$ the rate coefficient for charge exchange between ions and neutrals and n_n the neutral density.

For electrons the inertia term $\frac{\partial}{\partial z}(m_e n v_{e,\parallel}^2)$ can be neglected as well as electron momentum sources because of the small electron mass, and we are left with

$$\frac{\partial}{\partial z}p_e + enE = -m_e(v_e - v_i)\nu_{ei}n - 0.71n\frac{\partial kT_e}{\partial z} \quad (18)$$

If we solve equation 18 for the parallel electric field, we obtain Ohm's law as

$$E = \frac{j_\parallel}{\sigma_\parallel} - \frac{0.71}{e}\frac{\partial kT_e}{\partial z} - \frac{1}{en}\frac{\partial p_e}{\partial z} \quad (19)$$

where the parallel current density has been defined as $j_\parallel = en(v_i - v_e)$ and the parallel electric conductivity as derived assuming balance between electric and e-i friction force as $\sigma_\parallel = e^2n/(m_e\nu_{ei})$. In most cases one assumes local ambipolarity, $j_\parallel = 0$ such that for a deuterium plasma $v_e = v_i = v$. Otherwise, a current continuity equation is needed e.g. to describe cases where external currents are driven in biasing experiments (cf. also the discussion in [2], chapter 17).

Next we proceed to the energy conservation equation for ions, which is given as

$$\begin{aligned}\frac{\partial q_{\parallel i}}{\partial z} &= \frac{\partial q_{\parallel i,conv}}{\partial z} + \frac{\partial q_{\parallel i,cond}}{\partial z} \\ &= \frac{\partial}{\partial z}\left[\left(\frac{5}{2}T_i + \frac{1}{2}m_iv_i^2\right)nv_i - \kappa_{0i}T_i^{5/2}\frac{\partial T_i}{\partial z}\right] \\ &= envE + +Q_{in} - Q_{eq}, \end{aligned} \quad (20)$$

where we have decomposed the parallel heat flux into its convective and conductive part. The heat conduction coefficient $K = \kappa_{oi}T_i^{5/2}$ has a very strong temperature dependence, for ions we have for deuterium ions $\kappa_{oi} = 60$ to get with T_i in eV and $\partial T_i/\partial z$ in eVm^{-1} the conductive heat flux in Wm^{-2}. The term Q_{in} denotes the energy exchange between ions and neutrals during charge exchange processes,Q_{eq} is the energy transport from ions to electrons in Coulomb collisions.

For electrons we get accordingly

$$\begin{aligned}\frac{\partial q_{\parallel e}}{\partial z} &= \frac{\partial q_{\parallel e,conv}}{\partial z} + \frac{\partial q_{\parallel e,cond}}{\partial z} \\ &= \frac{\partial}{\partial z}\left[\frac{5}{2}T_env_e - \kappa_{0e}T_e^{5/2}\frac{\partial T_e}{\partial z}\right] \\ &= -envE + Q_r - Q_{ei} + Q_{eq}, \end{aligned} \quad (21)$$

.

Again we have omitted the inertia term in the convective flux, Q_r denotes the Joule heating term (not present if $j_\parallel = 0$), Q_{ei} is the energy loss of electrons because of inelastic collisions which ionize or excite neutrals. The heat conduction by electrons is substantially larger than that of ions, $\kappa_{oe} = 2000$, because of the $m^{-1/2}$ dependence of the heat conductivity.

Now we are still missing *boundary conditions* for our fluid equations 6, 15, 18, 20 and 21. At the stagnation plane we request from symmetry considerations

$$v_\parallel = \frac{\partial n}{\partial z} = \frac{\partial T_i}{\partial z} = \frac{\partial T_e}{\partial z} = 0. \quad (22)$$

The boundary conditions at the limiter and target plate are defined by the existence of the Debye sheath mentioned before, which is the subject of the next section.

VI. THE SHEATH

Within the Debye sheath quasi - neutrality is no longer fulfilled and the electrostatic potential is given by Poisson's equation

$$\frac{\partial^2 V}{\partial z} = -\frac{e}{\varepsilon_0}(n_i - n_e). \quad (23)$$

In this potential the electrons can be described by a Boltzmann equation

$$n_e(z) = n_{se}\exp(e(V - V_{se})/kT_e) \quad (24)$$

where $n_{se,e} = n_{se,i} = n_{se}$ is the density at the sheath entrance. This potential distribution constitutes a hill for the electrons ($V < 0$), as the limiter or divertor surface has initially been charged negatively by the electrons. At the sheath entrance we have the potential V_{se} which will be deduced from the parallel transport equations in section VII.

The ions will be accelerated in the sheath. If we assume now following the derivation in [2] that the parallel ion flux density remains constant within the very thin sheath, $n_iv_i = const.$, and for a moment that $T_i = 0$, we can use ion energy conservation $\frac{1}{2}m_iv_i^2 = -eV$ (no change of thermal energy) to obtain

$$n_i(z) = n_{se}(V_{se}/V)^{1/2}. \quad (25)$$

We use Eqns. 24 and 25 to transform 23 to

$$\frac{\partial^2 V}{\partial z} = -\frac{e}{\varepsilon_0}n_{se}\left[\left(\frac{V_{se}}{V}\right)^{1/2} - \exp(e(V - V_{se})/kT_e)\right]. \quad (26)$$

Now we consider the region just inside the sheath where $\Delta V \equiv V_{se} - V > 0$ is small with respect to V and expand the two terms on the RHS of Eqn. 26

$$\left(\frac{V_{se}}{V}\right)^{1/2} \approx 1 + \frac{1}{2}\frac{\Delta V}{V_{se}} = 1 - \frac{1}{2}\frac{\Delta V}{|V_{se}|} \quad (27)$$

$$\exp\left(e(V - V_{se})/kT_e\right) \approx 1 - \frac{e\Delta V}{kT_e} \quad (28)$$

to get

$$\frac{\partial^2 \Delta V}{\partial z} = \frac{e\Delta V}{\varepsilon_0} n_{se} \left(\frac{e}{kT_e} - \frac{\Delta V}{|V_{se}|} \right). \qquad (29)$$

From the condition that the electric potential in the Debye sheath has a monotonic distribution it follows that

$$\begin{aligned} \frac{e}{kT_e} &\geq \frac{\Delta V}{|V_{se}|} \\ m_i v_{se}^2 &\geq kT_e \\ v_{se} &\geq c_s \end{aligned} \qquad (30)$$

where c_s is the sound velocity and Eqn. 30 defines the *Bohm criterion* for the "plasma exit velocity". It will be supplemented with a condition $v_{se} \leq c_s$ following from the calculation of the parallel velocity profile in the SOL as described in section VII to end with $v_{se} = c_s$ as boundary conditions for the parallel flow at the sheath entrance (valid as long no drifts are considered, cf. section VIII).

Using this Bohm criterion we can describe the ion flux density to the target as the parallel flux density at the sheath entrance (se) (neglecting additional sources in the very thin sheath)

$$\Gamma^i_{target} = n_{es} c_s = \frac{1}{2} n(0) \sqrt{\frac{k(T_i + T_e)}{m_i}}. \qquad (31)$$

To preserve ambipolarity the ion flux (for an ion charge Z=1) must balance the electron flux which is influenced by the sheath potential drop V_s. The electron distribution remains Maxwellian in the retarding electric field. Thus, the electron flux to the target reads

$$\Gamma^e_{target} = \frac{1}{4} n_{es} \bar{c}_e = \frac{1}{4} n_{es} \exp\left(\frac{eV_s}{kT_e}\right) \sqrt{\frac{8kT_e}{\pi m_e}}. \qquad (32)$$

Equating 31 and 32 yields

$$\frac{eV_s}{kT_e} = 0.5 \ln\left(2\pi \frac{m_e}{m_i}\right)\left(1 + \frac{T_i}{T_e}\right). \qquad (33)$$

Typical values for the ratio given above are about 3. To quantify the total potential drop between stagnation plane and target surface one has to add the pre-sheath potential drop deduced in the next section VII (cf. Eqn. 48). Emission of electrons from the surface reduces the electrostatic potential. In some cases it can even lead to a breakdown of the sheath. The most important effect is the emission of secondary electrons, but also reflected electrons, photon induced emission and thermal emission play a role. In particular, above certain temperatures thermal emission can dominate and is considered to be one reason for the formation of so called hot spots [16].

The ions gain energy in the sheath (at the expense of the electrons which are cooled because only the fast part of the electron population can leave the plasma while the slower ones are repelled by the sheath potential). The impact energy of ions to the target

$$E_{ion} = 2kT_i + 3ZkT_e \qquad (34)$$

with Z the charge of the ions, is significantly increased by the acceleration in the sheath, especially for highly charged impurity ions, leading to enhanced physical sputtering (cf. discussion in [1]).

The heat flux density of ions and electrons from the plasma onto the surface can be related to the particle flux densities leaving the plasma with the help of the so called "sheath transmission coefficients" defined as

$$\gamma_{i,e} = \frac{q_{i,e}}{kT_e \Gamma_{target}} \qquad (35)$$

For electrons we get $\gamma_e \approx 2 + 3 + 0.5$ from the thermal, sheath and pre- sheath contribution. The ions don't have a Maxwellian distribution, if they had, then $\gamma_i \approx 2.5T_i/T_e + 0.5 + 0.5T_i/T_e$. Numerical simulations allowing for non- Maxwellian ion distributions give somewhat smaller results $\gamma_i \approx 2 - 3$. The total sheath transmission coefficient is then around $\gamma = 8$. The heat flux density to the target can be expressed as

$$q_{target} = \gamma n_{es} c_s k T_e = n_{es} \sqrt{\frac{k(T_i + T_e)}{m_i}} kT_e. \qquad (36)$$

We finally can include the power flow deposited on the target upon recombination of the ion-electron pairs and possibly formation of molecules. This potential energy flow density can be expressed as

$$q_p = n_{es} c_s k \varepsilon_p = n_{es} \sqrt{\frac{k(T_i + T_e)}{m_i}} \varepsilon_p. \qquad (37)$$

with the potential energy ε_p composed of the ionization and dissociation energy of deuterium atoms and molecules, $\varepsilon_p \approx 16eV$.

The magnetic field $\overrightarrow{B}$ has no influence on the sheath description as long as the surfaces are orthogonal to $\overrightarrow{B}$. In practice, however, surfaces are tilted to spread the power onto the target. By enlarging the angle Ψ between $\overrightarrow{B}$ and the normal to the surface the power flux density normal to the target can be reduced to

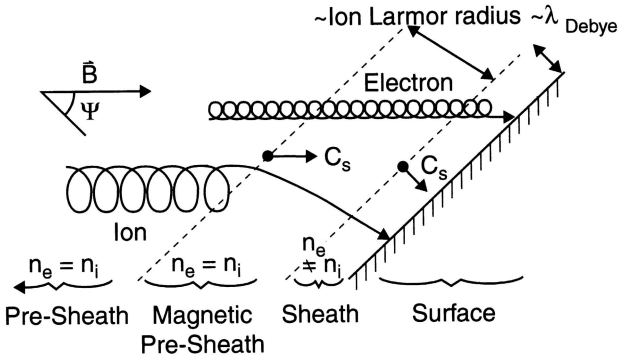

Figure 4: Near surface region for a target inclined to the magnetic field [11] (figure adapted from [2])

$$q_{dep} = q_{\parallel} \cos \Psi. \tag{38}$$

The parallel heat flux density in a fusion reactor can be in the order of $100 - 1000 MW m^{-2}$ so that a shallow inclination of the targets with Ψ up to 89^o is envisaged. For these small angles of incidence a new feature, the *magnetic pre-sheath* [11] shows up, which extends from the electrostatic Debye sheath discussed before about one ion larmor radius ($\sim 10^{-3} m$) into the plasma. The reason for the formation of the magnetic pre- sheath is, that there is now an ExB drift of the ions perturbing the last gyro-orbits in front of the target, while the electrons will follow the magnetic field lines virtually all the way to the surface because of their much smaller gyro radius (cf. fig. 4). As a consequence, the Bohm criterion for the parallel flow now applies at the magnetic pre- sheath edge.

Equating the ion flux at the magnetic pre- sheath (mse) with the electron flux at the electrostatic sheath entrance (se), again assuming ambipolar flow and no sources in the pre-sheath and the Boltzmann relation for electrons)

$$n_{mse} c_s \cos \Psi = n_{se} c_s = n_{mse} \exp\left(eV_{mse}/(kT_e)\right) c_s \tag{39}$$

leads to

$$\frac{eV_{mse}}{kT_e} = \ln \cos \Psi. \tag{40}$$

The total potential drop in Debye V_{DS} and magnetic pre-sheath V_{mse} together is independent on Ψ to first order as found in numerical calculations [11], instead Ψ determines the split between V_{mse} and V_{DS}. Thus, to first order, the sink action of the solid surface acting on the plasma, with regard to both particle and power flows, is unaffected by the change from a normal to an oblique target, as are the sheath voltage drop and the ion impact energy onto the target (Eqn. 34).

VII. PROPERTIES OF THE SIMPLE SOL

Now we return back to the description of the parallel flow in the SOL. First we will describe the case of the simple SOL (cf. fig. 2a), which is also called the *sheath- limited regime*. The model assumptions are the following:

- The 1D fluid flow is isothermal, $T_i = const.$ and $T_e = const.$, and there are no heat sinks or sources inside the SOL. Thus, we don't need the energy transport equations.
- There are no particle sources from ionization inside the SOL, the only source is diffusive cross field transport.
- The target is a perfect plasma sink, there are no volume sinks as recombination.
- The ions and electrons are fully decoupled.

The source term for the continuity equation along z is given by radial particle transport into the SOL (no ionization inside the SOL)

$$\frac{\partial}{\partial z}(n v_{\parallel}) = S_p = -\frac{\partial}{\partial x}(D_{\perp} \frac{\partial n}{\partial x}) = \frac{D_{\perp} n}{\lambda^2}. \tag{41}$$

For the ion momentum balance, we again neglect friction with neutrals (CX losses and ionization) and represent the electric field with the help of the Boltzmann relation Eq. 24 yielding

$$m_i n v_{\parallel} \frac{\partial v_{\parallel}}{\partial z} = -k(T_e + T_i) \frac{\partial n}{\partial z} + m_i v_{\parallel} S_p \tag{42}$$

with S_p as given by Eq. 41.

Defining a parallel Mach number $M_{\parallel} = v_{\parallel}/c_s$ and using the definition of the (isothermal) ion sound velocity $c_s = \sqrt{(k(T_e + T_i)/m_i}$ we can now use Eqs. 41 and 42 to deduce two coupled equations which describe the variation of the density and the Mach number along z

$$\frac{\partial n}{\partial z} = -\frac{n D_{\perp}}{c_s \lambda^2} \frac{2 M_{\parallel}}{1 - M_{\parallel}^2} \tag{43}$$

$$\frac{\partial M_{\parallel}}{\partial z} = \frac{D_{\perp}}{c_s \lambda^2} \frac{1 + M_{\parallel}^2}{1 - M_{\parallel}^2} \tag{44}$$

The divergence of these two equations for $M_{\parallel} = \pm 1$ defines the boundary condition of the flow at the sheath

entrance (the Bohm criterion as mentioned before). Combining Eqs. 43 and 44 we get

$$\frac{\partial n}{\partial M_\parallel} = -n\frac{2M_\parallel}{1+M_\parallel^2} \tag{45}$$

which can be integrated analytically:

$$\frac{n}{n_0} = \frac{1}{1+M_\parallel^2} \tag{46}$$

with n_0 the density in the stagnation plane where $M_\parallel(z=0)=0$. Therefore, the density drops from the stagnation point to the sheath entrance to half its value. As we assumed no variation of the particle source originating from cross field transport into the SOL and $|\partial n/\partial x| = n/\lambda = const.$, the SOL thickness λ reduces towards the target proportional to the density further aggravating the problem of the high target load as indicated before.

The equation describing the variation of the Mach number along z reads

$$M_\parallel - 2\arctan M_\parallel = (\frac{\pi}{2}-1)\frac{z}{L} \tag{47}$$

Finally, combining Eq. 46 and 24 we get an equation for the potential in the pre-sheath

$$V(z) = -\frac{kT_e}{e}\ln(1+M_\parallel(z)^2) \tag{48}$$

Therefore, at $M_\parallel = 1$ the total pre-sheath drop is given by $V \approx -0.69kT_e/e$.

Fig. 5 depicts the variation of the plasma density, the Mach number and the electric potential as given by Eqs. 46, 47 and 48, respectively, from the stagnation plane z/L=0 to the sheath entrance z/L=1.

For the situation of a simple SOL the power flux density is determined by the power flow into the SOL and the power decay length together with the perpendicular extension of the target (i.e. the poloidal extension in case of a toroidal limiter), which is small as is the density decay length discussed in section III. At the same time the temperature at the target surface remains high, unless both the power flow into the SOL and the temperature at the LCFS are reduced by power loss mechanisms inside the confined volume (in this context the concept of radiation cooling will be introduced in section X).

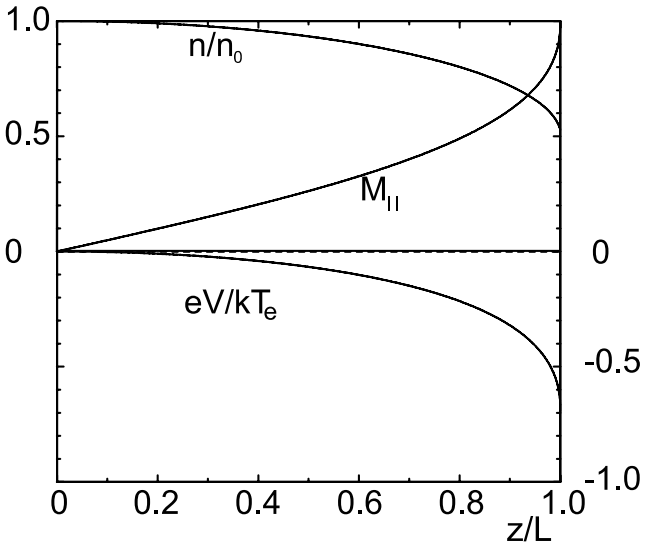

Figure 5: Variation of plasma density n normalized to n(0), parallel Mach number and normalized potential drop in the pre- sheath along the magnetic field from the stagnation plane z/L=0 to the sheath entrance z/L=1

VIII. IMPACT OF DRIFTS ON THE SOL FLOW

Next we discuss briefly the influence of drift effects on the parallel particle transport in the SOL which have been identified as the cause of significant poloidal asymmetries in tokamaks ([12], [13], [14], [15], cf. also discussion in [2], chapter 18, and references therein).

The model for the parallel transport discussed before can be extended to include a perpendicular drift component caused by ExB drift, diamagnetic drift and ∇B and curvature drift. We decompose the drift motion into a radial and a binormal component ($\vec{e}_r \perp \vec{e}_\perp \perp \vec{e}_\parallel$) which allows to express the poloidal velocity component v_θ as

$$v_\theta = v_\parallel \sin\alpha + v_\perp \cos\alpha \tag{49}$$

where α denotes the angle between the toroidal and poloidal magnetic field components as before ($\tan\alpha = B_\theta/B_\phi$)).

As we will continue to investigate transport along the field line, we have to project the resulting poloidal velocity onto the parallel direction (cf. fig. 6)

$$\tilde{v}_\parallel = v_\parallel + \frac{1}{\tan\alpha}v_\perp. \tag{50}$$

As a consequence Eqs. 43 and 44 are modified to

$$\frac{\partial n}{\partial z} = \frac{nD_\perp}{c_s\lambda^2}\frac{2M_\parallel + M_\perp/\tan\alpha}{(M_\parallel + M_\perp/\tan\alpha)^2 - 1} \tag{51}$$

$$\frac{\partial M_\parallel}{\partial z} = \frac{D_\perp}{c_s\lambda^2}\frac{1+(M_\parallel + M_\perp/\tan\alpha)^2}{1-(M_\parallel + M_\perp/\tan\alpha)^2} \tag{52}$$

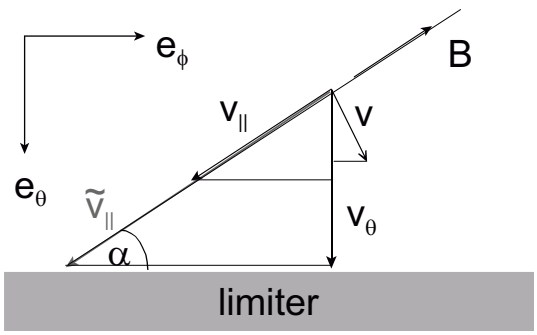

Figure 6: Projection of the perpendicular drift velocity onto the parallel direction.

where $M_\perp$ normalizes the perpendicular velocity to the sound speed. The boundary condition for the parallel Mach number at the sheath entrance reads

$$M_\parallel(z = \pm L) = \pm 1 - \frac{M_\perp}{\tan\alpha}. \qquad (53)$$

Consequently, the flow towards both sides of the limiter or to the two divertor plates shown in Fig. 1 is asymmetric, resulting in an asymmetric density distribution along the field line and in poloidal direction. Eq. 46 is replaced by

$$\frac{n}{n_0} = \frac{1}{1 + M_\parallel(M_\parallel + M_\perp/\tan\alpha)}. \qquad (54)$$

Within the simple model discussed above (still under the assumptions of no ionizations in the SOL) Fig. 7 illustrates the influence of a perpendicular Mach number $M_\perp = 0.05$ on the parallel Mach number along the field line from the electron drift side of the ALT- II limiter in TEXTOR (located 45^0 below the outer midplane) to the ion drift side. The toroidal magnetic field and plasma current are anti- parallel under standard conditions in TEXTOR. In that case $M_\parallel > 1$ on the ion drift side. The stagnation plane (as defined by $M_\parallel = 0$) is considerably shifted away from the geometrical symmetry plane (located at $z = 0.5$; here we normalize z to the total length of the flux tube $2L$).

In poloidal divertor tokamaks drifts are thought to be the cause of strong asymmetries in the power load of inner and outer divertor target plates, so that both divertor zones are often in different divertor regimes. These divertor regimes are the topic of the following section.

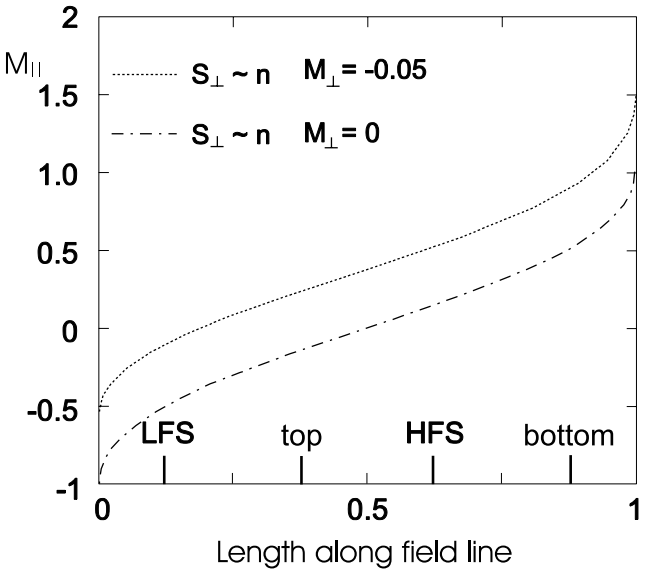

Figure 7: Influence of a perpendicular drift on the parallel Mach number($\tan\alpha = 0.1$, no ionization in the SOL)

IX. PROPERTIES OF THE COMPLEX DIVERTOR SOL

At the end of section VII we have noted the problems of high power flux densities and high temperatures in limiter SOLs. While the high power flux densities lead to large temperatures of the surfaces of plasma facing components, high temperatures give rise to large energies of particles impinging onto the material surface (cf. Eqn. 34). Both effects will pose huge problems with the plasma- wall interaction in fusion devices (see [1]). Therefore, the formation of a plasma regime with reduced power flow to and a cold plasma in front of the targets *(conduction limited and high recycling regime)* is an important issue in plasma edge physics.

The possibility to reduce the plasma temperature in front of the plasma facing components by establishing a temperature gradient along the magnetic field lines is closely related with the necessity to localize the ionization of neutrals close to the target. As it is depicted in fig. 2b) the parallel plasma flow is then only developing in the ionization (or recycling) region close to the target, most of the SOL is stagnant. In particular, there is no particle flux into the SOL from the confined volume. In practise, such a situation cannot be reached to a full extend because there will be also interaction of the plasma with the main chamber walls, leading to ionization sources remote from the divertor target or limiter inside the SOL or even sources in the confined plasma, if the neutrals recycling at the main chamber walls penetrate across the LCFS. Nevertheless, the particle flux from the core and into the SOL remote from the targets may be rather small with respect to the re-

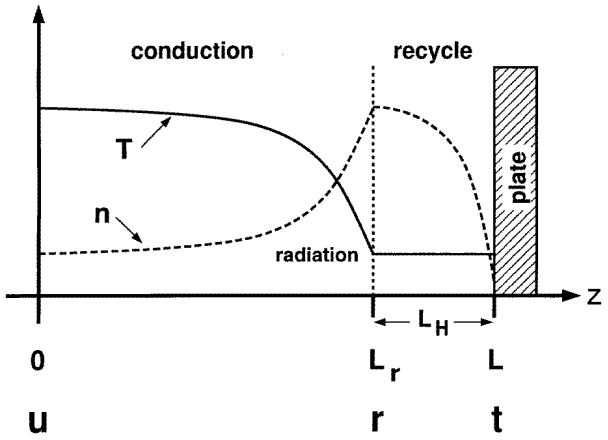

Figure 8: Schematic illustration of the two point model (figure adapted from [5])

cycling flux at the targets. While the particle sources are close to the targets, the heat fluxes remain in the core of the confined plasma. Therefore, there is still the power flow out of the confined volume into the SOL and along the magnetic field towards the targets which constitute the heat sink. Without particle flow this heat flux cannot be convective but will be conductive and a temperature gradient *must* develop.

We can quantify the effects in the complex SOL of a divertor using a simple analytical model (the so called "two point model", cf. [2], chapters 4 and 5, and [5]). For simplicity we assume equal ion and electron temperatures, $T_i = T_e$. Fig. 8 illustrates the typical plasma profiles along the magnetic field for such a situation. We have two different regions, the conduction region consisting of most of the SOL where there are no sources or sinks, and the recycling region where we have the strong ionization sources and possibly a sink for energy and momentum. The two point model relates the conditions upstream of the target (position u) to those at the target (position t) in the case where the fraction f_{cond} of the power is conducted along the parallel temperature gradient as

$$q_{||,cond} = f_{cond} P_{SOL}/A_{q||} = -\kappa_0 T^{5/2} dT/dz, \quad (55)$$

where κ_0 is taken for electrons because of their higher heat conductivity (cf. Eqns. 20 and 21), P_{SOL} is the power flow into the SOL and $A_{q||}$ the total cross-sectional area of the SOL for power flow perpendicular to $\overrightarrow{B}$ (all power enters the SOL upstream of the target). We include possible volumetric power sinks characterized by the factor $f_{loss} > 0$ in the balance between power flux into the SOL and power flux at the sheath entrance as

$$(1 - f_{loss}) P_{SOL}/A_{q||} = \gamma n_t c_s k T_t \quad (56)$$

We further introduce a factor $f_{fric} < 1$ into the pressure balance to take pressure losses because of momentum sinks and friction into account

$$n_u T_u f_{fric} = 2 n_t T_t. \quad (57)$$

Momentum losses induced by CX processes between ions and neutrals in a high density divertor play a major role in in poloidal divertors and occur for very low temperatures below 7 eV, and we will come back later to an assessment of the factor f_{fric}. On the other hand, in the island divertor of helical devices detachment processes at higher temperatures have been observed, which have been related to friction losses caused by counter streaming flux tubes in the complicated 3D geometry of such an island divertor [28] [7]. An expression for $f_{fric,CX}$ has been been given in [5] following an 1D analytical solution for the momentum balance in [29]. Here it is assumed that the temperature in the recycling region shown in fig. 8 is constant and the momentum loss reduces the density only. The density ratio between the entrance of the recycle region (r) and the target is given as

$$\frac{n_r}{n_t} = \left(\frac{\alpha+1}{\alpha}\right)^{(\alpha+1)/2} \quad (58)$$

where the coefficient α is linked to the rate coefficients for ionization and charge exchange (cf. section IV) as $\alpha \equiv < \sigma v >_i / (< \sigma v >_{CX} + < \sigma v >_i)$. Using the pressure balance equation 57 we obtain

$$f_{fric} = 2 \left(\frac{\alpha}{\alpha+1}\right)^{(\alpha+1)/2} \quad (59)$$

.

This Equation fairly well describes the experimentally determined pressure drop in the high density Alcator - CMOD tokamak [5] as shown in fig. 9.

Returning back to the two point model we now integrate Eqn. 55 over the distance L between the upstream region u and the target region t to obtain

$$T_u^{7/2} = T_t^{7/2} - \frac{7}{2} \frac{P_{SOL} L}{A_{q||} \kappa_0} f_{cond}. \quad (60)$$

Because $T_t^{7/2} \ll T_u^{7/2}$ as soon as a temperature gradient exists the upstream temperature is given as

$$T_u = \left(\frac{7}{2} \frac{P_{SOL} L}{A_{q||} \kappa_0} f_{cond}\right)^{2/7} \quad (61)$$

showing a very weak dependence on all parameters.

If we now take n_u and $P_{SOL}/A_{q||}$ as given, we can derive from Eqs. 56, 57 and 61 an expression for the temperature at the target

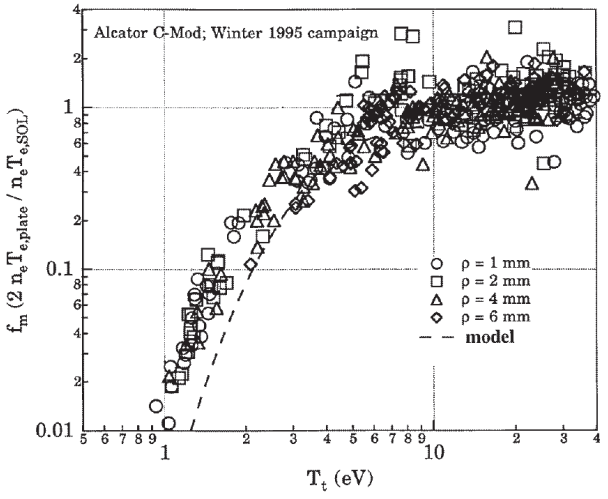

Figure 9: Pressure loss factor from ohmic discharges in C-Mod as a function of the electron temperature at the target T_t and factor calculated from Eqn. 59 (figure adapted from [5]).

$$T_t = \frac{m_i}{2e}\frac{4(P_{SOL}/A_{q||})^2\left(\frac{7}{2}\frac{P_{SOL}L}{A_{q||}\kappa_0}\right)^{-4/7}}{\gamma^2 e^2 n_u^2}\cdot\frac{(1-f_{loss})^2}{f_{fric}^2 f_{cond}^{4/7}}. \quad (62)$$

Correspondingly we get for the density n_t at the target

$$n_t = \frac{n_u^3}{(P_{SOL}/A_{q||})^2}\left(\frac{7}{2}\frac{P_{SOL}L}{A_{q||}\kappa_0}\right)^{6/7}\frac{\gamma e^2}{2m_i}\cdot\frac{f_{fric}^3 f_{cond}^{6/7}}{(1-f_{loss})^2}. \quad (63)$$

High upstream densities n_u are very efficient to realize a cold and dense high recycling divertor with high n_t and low T_t. We further note that the plasma conditions at the target depend very sensitively on the loss parameters f_{loss}, f_{cond} and f_{fric}. A consistent picture of these parameters can only be obtained from sophisticated modelling (cf. the discussion in [4]).

Nevertheless, we will give some further considerations on the balance between convective and conductive heat flux density, which determines the desired temperature drop along the field lines.

As a first step we can deduce the ratio between upstream and target temperature from Eqn. 61 and 62 which scales as

$$\frac{T_u}{T_t} \propto n_u\left(\frac{7}{2}\frac{P_{SOL}L}{A_{q||}\kappa_0}\right)^{6/7}\frac{f_{fric}^2 f_{cond}^{6/7}}{(1-f_{loss})^2}. \quad (64)$$

Naturally, the existence of conductive heat transport ($f_{cond} > 0$) and the resulting temperature ratio is directly linked, and any contribution heat convective heat transport will reduce T_u/T_t. Volumetric power losses close to the target strongly drive the temperature drop but momentum losses impede it. But what is now the ratio between convective and conductive heat flux and how to control it? Why we observe high recycling regimes in divertor configuration but not in limiter machines? This difference is of course strongly linked to the possibility to retain the ionization sources inside of the SOL. To quantify this statement we have integrated the balance equation for the total energy (sum of Eqns. 20 and 21) retaining both conductive and convective heat flux densities. We used the power flux density as well as the particle flux density to the target as a boundary condition. The convective heat flux is driven by the particle sources inside the confined plasma $f_{SOL}\Gamma_0$ where we assume complete recycling at the target, $\Gamma_{t,\|} = \Gamma_0$. We obtain

$$\begin{aligned}\frac{\partial q_\|}{\partial z} &= \frac{q_{\|,t}}{L} \\ &= \frac{\partial}{\partial z}q_{\|,cond} + \frac{\partial}{\partial z}q_{\|,conv}. \end{aligned} \quad (65)$$

Here we have the parallel heat flux to the target given by the power P_{SOL} entering the SOL all along the connection length L, the cross section of the heat flux channel $A_{q\|} = 4piR\lambda_{q\|}a/(q_a R)$ and the energy loss by ionization and excitation $E_i = 30eV$ [3] given as

$$q_{\|,t} = \frac{P_{SOL}}{A_{q\|}} - f_{SOL}\Gamma_0 E_i = \gamma\Gamma_{t,\|}kT_t \quad (66)$$

and the rate of change of the conductive and convective heat flux density given as

$$\begin{aligned}\frac{\partial}{\partial z}q_{\|,cond} &= -\kappa_{e0}\left[T^{5/2}\frac{\partial^2 T}{\partial z^2} + \frac{5}{2}T^{3/2}\left(\frac{\partial T}{\partial z}\right)^2\right] \\ \frac{\partial}{\partial z}q_{\|,conv} &= (1-f_{SOL})k\frac{\Gamma_0}{L}\left(5T + z\frac{\partial T}{\partial z}\right). \end{aligned} \quad (67)$$

The second order differential equation 65 is solved for T numerically after transformation into two first order equations

$$\begin{aligned}\frac{\partial T}{\partial z} &= \tilde{T} \\ \frac{\partial \tilde{T}}{\partial z} &= -(\kappa_{e0}L)^{-1}T^{-5/2}\left[q_{\|,t} - \frac{\Gamma_0}{(1-f_{SOL})k}(5T + z\tilde{T})\right] \\ &\quad -\frac{5}{2}\tilde{T}^2 T^{-1} \end{aligned} \quad (68)$$

The boundary conditions are

$$\frac{\partial T}{\partial z}|_{z=0} = 0 \ \text{ and } \ T|_{z=L} = T_t\,. \quad (69)$$

The target temperature is defined by the inferred heat flux density to the target Eqn. 66. The target density follows from the particle flux to the target, and target temperature and the upstream densities and temperatures are determined by the pressure balance Eqn. 57 where no momentum losses are considered.

We use typical parameters for the limiter tokamak TEXTOR, major radius $R = 1.75m$, minor radius $a = 0.46m$, connection length $L = 20m$, edge safety factor $q_a = 3$, power entering into the SOL $P_{SOL} = 1MW$, power decay length $\lambda_{q\|} = 0.02m$ and vary then the particle flux density onto the target. We use the fraction of ionizations inside the SOL f_{SOL} as a parameter. The results are shown in fig. 10.

We scanned the collisionality $\nu_* = L/\lambda_{ee}$ as the ratio between the connection length and the mean free path of electrons (or ions) in a wide range and calculated the ratio of upstream and target temperature T_u/T_t, absolute values of upstream and target temperatures, T_u and T_t as well as fraction of power lost on ionization and excitation of neutrals in the SOL f_{loss}. The calculation is stopped as soon as the target temperature approaches a value of $7eV$ because at these temperatures momentum dissipation by CX processes will become significant. We clearly see that the fraction of ionizations in the SOL has to be 0.6 and higher to allow for a significant temperature drop along the magnetic field. Such large neutral screening is, however, inaccessible in a limiter device because neutrals recycling at the limiter penetrate into the confined zone even at highest densities when the temperature falls below the ionization threshold for hydrogen.

Our result is consistent with [30] where an improved two point model including both convective and conductive heat transport as well as a realistic description of the neutrals and the resulting particle sources had been developed for a limiter SOL and compared to full numerical simulations with a fluid code coupled to a Monte-Carlo code for the neutrals (both codes use full 3D geometry). Here the numerical code shows that at maximum 50% of the neutrals can be ionized in the SOL of TEXTOR. As a consequence, the ratio T_u/T_t saturates at high collisionality. Higher neutral screening is only possible in a divertor tokamak where the targets are positioned remote from the confined volume inside. Closed divertor configurations which suppress leakage of neutrals out of the divertor chamber are best in this respect (cf. also the discussion in [4]).

As we see from fig. 10 under conditions of good neutral screening from the divertor we quickly approach a situation, where the temperatures in the recycling region are small enough to allow for large momentum losses, leading to a *detached* divertor state. Then the particle and power flux to the divertor plate is strongly

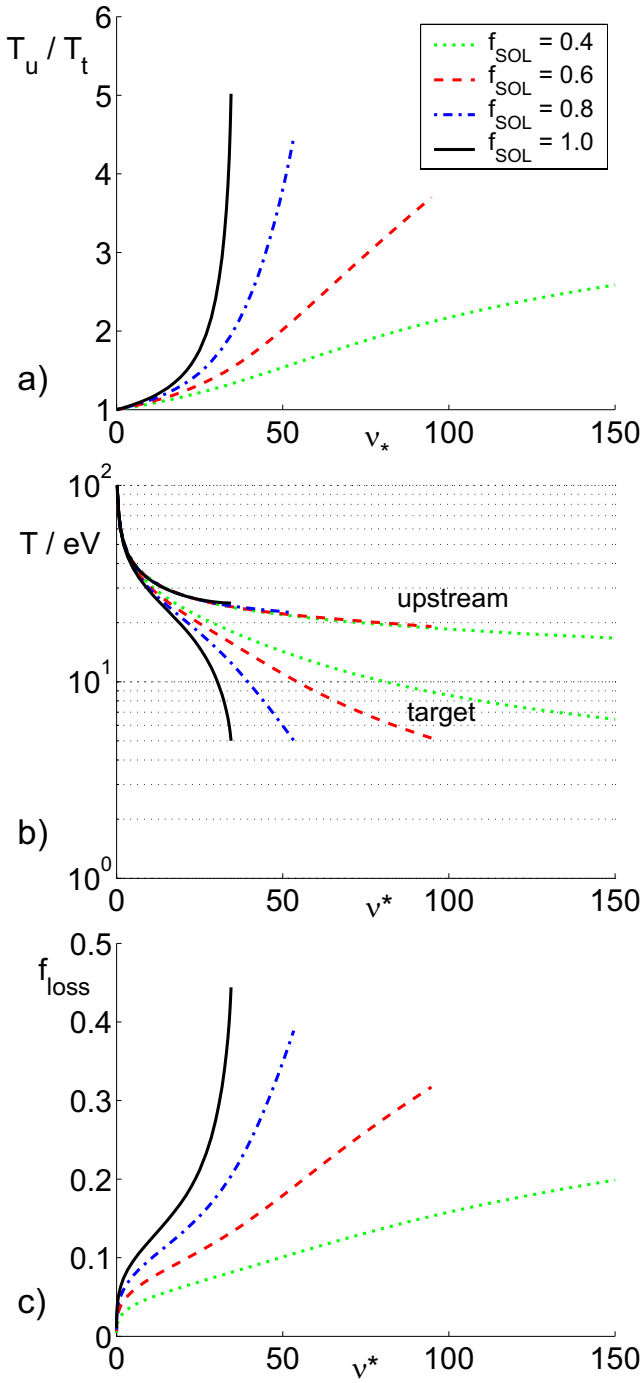

Figure 10: Variation of SOL parameters as a function of the upstream collisionality for typical TEXTOR conditions using the fraction of ionizations inside the SOL as parameter: a) ratio of upstream and target temperature, b) absolute values of upstream and target temperatures, b) fraction of power lost on ionization and excitation of neutrals in the SOL

reduced. Such a regime is envisaged for fusion devices. However, stability of a detached divertor is an issue as we can expect from the complicated and non-linear interplay of the various loss channels. Also the need for additional losses by radiation from impurities is a subject of current research. In present days experiments the high heat load areas of the divertors are mostly made of carbon, an effective intrinsic radiator at the low temperatures close to detachment (see the extensive discussion in [4]). We will review some basics of impurity transport and radiation in divertor in the next section.

X. IMPURITY TRANSPORT AND RADIATION AT THE PLASMA EDGE

The physics of impurity transport and radiation in the plasma edge of fusion is importance because of two main reasons. *At first* the impurities eroded from plasma facing components and entering the plasma core will lead to radiation losses and fuel dilution in the plasma volume where the fusion processes shall take place, as a consequence the operational range to access a given fusion gain is reduced. The degree to which the impurities are present in the fusion volume depends on three aspects: the source strength of impurities (the influx rate) which is governed by the plasma- surface interactions processes ([1]), the penetration of the impurity neutrals into the edge and the resulting ion source distribution inside and outside the SOL and the radial transport of impurities in core. Experiments and modelling have shown, that the first two aspects are of large importance (cf. discussion in [2], chapter 6).

Secondly, the line radiation of impurities can provide a tool to exhaust the power from fusion plasmas to large areas which otherwise are concentrated by the parallel heat flux in the SOL to small areas at the plasma facing components as described in the previous section.

The total radiation consists of three contributions: line radiation, bremsstrahlung and recombination radiation. At the plasma boundary the main contribution is given by line radiation caused by radiative transitions between different atomic energy levels of the various ionization stages. The local radiated power density p^z_{rad} of an impurity ion with charge state z is expressed with the help of a cooling rate L_z as

$$p^z_{rad} = n_e n_z L_z \qquad (70)$$

where n_e and n_z denote the local densities of electrons and the impurity ionization stage under consideration. Here the electron density enters as the excited levels of the impurity ions are populated via inelastic

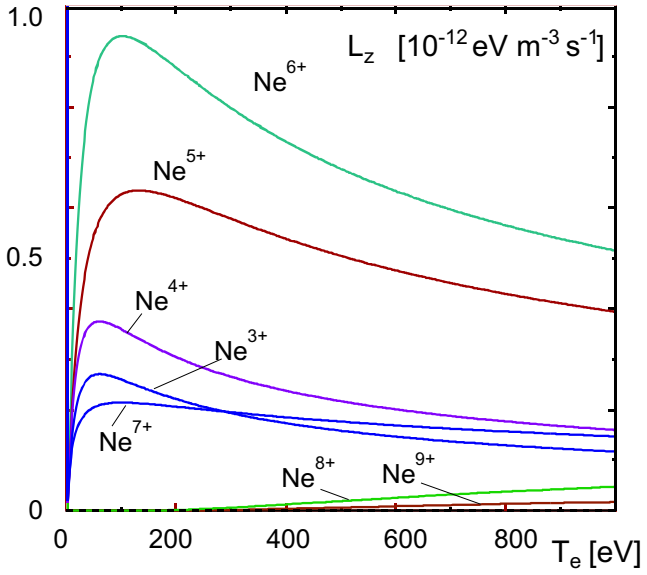

Figure 11: Cooling rates of different neon ionization stages

electron collisions for plasma conditions which are typical for magnetically confined fusion plasmas. For very low densities as they are typical for the solar corona, the population via collisions is balanced by radiative decay and the population densities of excited states are small with respect to the ground states (so called coronal (excitation) equilibrium). Then the cooling rate L_z is given by the product of the rate coefficient $< \sigma v >^{ex}_{1k} (T_e)$ for electron impact excitation (a function of the electron temperature for a Maxwellian velocity distribution of electrons) and the energy difference ΔE_{1k} between ground state and excited state k where we have to sum over all excited states.

$$L_z(T_e) = \sum_k < \sigma v >^{ex}_{1k} (T_e) \Delta E_{1k}. \qquad (71)$$

More generally the population of ions in the plasma boundary of fusion plasmas has to be determined by a collisional radiative model where also collisional de- excitation is taken into account. Consequently, the cooling rate is depending on both electron temperature and density. Cooling rates of various fusion relevant impurity species can be deduced from the ADAS package [24]. To be used in impurity transport models the cooling rates determined from Eqn. 71 are parameterized for an efficient calculation and given as functions of T_e. Fig. 11 shows the cooling rates of various ionization stages of neon. It can be seen in Fig. 11 that the Helium and Hydrogen like ionization stages are characterised by much lower cooling rates than the lower stages.

More extended descriptions of radiation processes

in plasmas can be found in [25] [26] [27] and more recently in [31].

To describe the radiated power losses the radial distribution of the different ionization stages is needed as determined by the particle balance equation

$$\frac{\partial n_Z}{\partial t} + \nabla \cdot \vec{\Gamma}_Z = \frac{n_{Z-1}}{\tau_{ion}^{Z-1}} - \frac{n_Z}{\tau_{ion}^{Z}} + \frac{n_{Z+1}}{\tau_{rec}^{Z+1}} - \frac{n_Z}{\tau_{rec}^{Z}} \quad (72)$$

which takes into account the time variation of densities, divergence of particle flows $\vec{\Gamma}_Z$, sources and sinks due to ionization and recombination with characteristic times τ_{rec}^Z through different channels, e.g., radiative, dielectronic recombination or charge exchange with hydrogen neutrals.

While for the confined volume radial transport is essential to determine the spatial distribution of impurity ions (with exceptions for low ionization stages which are ionized before the get uniformly distributed on a magnetic flux surface), in the divertor SOL in particular parallel transport has to be considered.

A. Impurity transport in the SOL and divertor radiation

We start with the transport of impurities in the SOL. In fact, the concept of divertors has been introduced with the primary hope to get a proper retention of the impurities inside of the divertor volume because of the separation between interaction zone (the divertor plates) and the confined region in divertor geometry (cf. fig. 1). In a simplified model the impurities are released from the divertor plates, penetrate into the divertor volume and are then transported along the field lines upward until the friction with the flow of the background ions flushes the impurities back to the target. However, there are also forces which push the impurities out of the divertor volume, so that the distribution is governed by the balance between these forces.

The force onto an impurity ion of charge state Z and density n_z along the field lines is given by

$$\begin{aligned} F_z = & - \frac{1}{n_z}\frac{\partial p_z}{\partial z} + m_z \frac{v_i - v_z}{\tau_s} + ZeE \\ & + \alpha_e \frac{\partial kT_e}{\partial z} + \beta_i \frac{\partial kT_i}{\partial z.} \end{aligned} \quad (73)$$

The first term at the RHS denotes the impurity pressure gradient force which drives the particle down the gradient, the second term is the friction force of the impurities with their flow velocity v_i exerted by the flow of the background (i.e. the contribution hoped for to retain the impurities in the divertor). The third term is the electric force in the parallel electric field. Generally it will attract the ions in the pre- sheath region, however strong local impurity sources in the SOL may produce reversed electric fields. The forth and fifth term are related to the temperature gradient of ions and electrons which are present in a conduction limited divertor regime. These contributions can actually pull out the impurities from the divertor. For $m_z \gg m_i$ the coefficients are given by $\alpha_e = 0.71Z^2$ and $\beta_i = 2.6Z^2$. Also the temperature gradient forces are are caused by collisions and arise because of the decrease of the collision frequency with temperature.

If we now consider typical plasma profiles in a divertor as depicted in fig. 8, we can distinguish three typical regions as sketched in fig. 12 (figure and description from [2]).

Region A, which is closest to the target, extents up to $z = s_{inj}$ where s_{inj} is the penetration depth of the impurity neutrals. Further upstream in region B, the density profile decays up to the end of the recycling region at $z = s_v$. Further out of the divertor we reach the region where we have substantial temperature gradients but no more background flow pushing the impurities back to the target plate. From here on the impurities will be pulled out of the divertor, leading to a "divertor leakage".

Impurity divertor radiation can effectively contribute to the formation of a cold divertor because it lowers the parallel heat flux entering the recycling region and thereby favors the onset of momentum detachment. In ASDEX- upgrade it could be shown that in a closed divertor geometry (Lyra Divertor) with carbon as intrinsic impurity even at high power fluxes almost all power can be dissipated in the divertor before it reaches the target plate, while a more open divertor configuration does not allow for high divertor radiation (see [4] and references therein.) However, the use of carbon as divertor radiator can be a problem in future fusion devices because of the co-deposition of tritium in carbon deposits at remote areas (cf. [1]). Therefore, the use of extrinsic impurities (noble gases like neon) are considered, although they will probably cause also more radiation from the edge of the confined plasma because of their higher Z.

B. Impurity radiation from the edge of the confined volume

To solve the problem of power exhaust from fusion plasmas the *concept of a cold radiating plasma mantle* has been proposed [36] [37]. Within this concept the power flux out of the plasma is distributed to large areas by photons, which are not affected by the magnetic field. The radiation losses originate from line radiation of impurities at the plasma periphery *inside* the confined volume which are - intentionally and in a re-

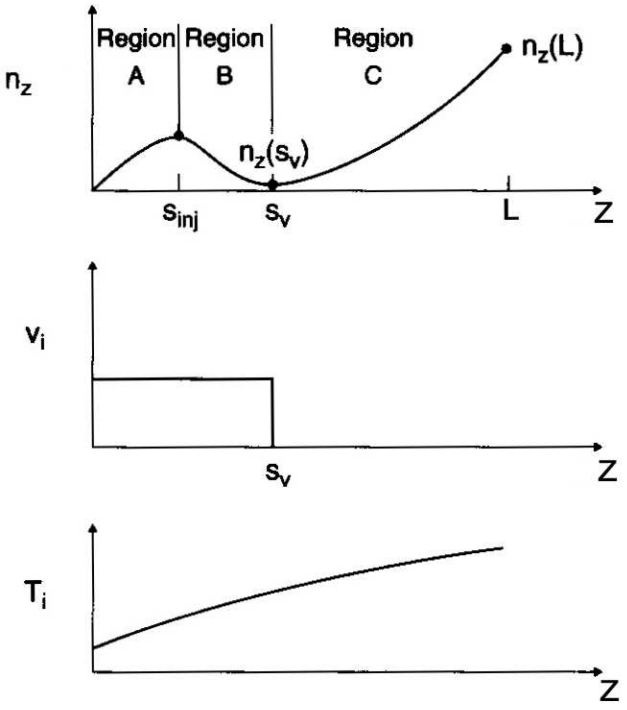

Figure 12: Characteristic impurity density profile in a conduction limited divertor with a temperature gradient along the magnetic field, the velocity profile of the background ions is approximated with a step function (adapted from [2]).

stricted manner - injected into the plasma discharge.

The application of such a concept to a fusion reactor is restricted to the degree to which different requirements can be met simultaneously:

- The concentration of injected impurities must be high enough to allow a high fraction of the total input power to be radiated from the edge. It has to be controllable at a stationary level.
- The line radiation has to be restricted to the plasma periphery. The impurity concentration in the inner plasma bulk where the fusion process takes place, must be limited to avoid too a strong fuel dilution or too high energy losses owing to radiation.
- The distribution of the power flux to large areas by radiation must still allow for a localisation of the particle flux which is sufficient for helium exhaust.
- The presence of the radiating impurities should not affect the magneto- hydrodynamic plasma stability, the energy confinement must not be diminished and the operation of the radiating plasma regime must be compatible with high fuel densities.

The first experimental proof of this concept in a tokamak plasma with reactor relevant heat flux densities and stationary operational conditions was demonstrated at the TEXTOR device in Jülich using feedback controlled neon injection to provide the cold radiating plasma mantle [38] [39]. Later on, condensing species like silicon have been investigated [40]. The compatibility with helium exhaust has been examined [41] and detailed calculations of the influence of radiating impurities on the power balance in a fusion reactor were done [42]. Moreover and in contrast to the common believe, the energy confinement is not degraded in discharges with a radiating boundary, but can even be improved as was found in the Radiative Improved Mode at TEXTOR [43].

In this context the radial flux of impurities in the plasma boundary is essential. It can be decomposed into a diffusive and convective term and given as

$$\Gamma_{\perp}^{Z} = -D_{\perp}\frac{\partial n_Z}{\partial r} + v\, n_Z \qquad (74)$$

As a consequence of the fluxes and different to the situation in the solar corona the ionization stage distribution is *not* solely determined by the electron temperature governing ionization and recombination rate coefficients. In corona equilibrium a total cooling rate $L(T_e)$ can be used which takes into account the ionization stage distribution governed by the RHS of Eqn. 72 only, and the total radiation losses follow from the product of total impurity density, electron density and total cooling rate. A compilation of total cooling rates for all fusion relevant elements under the assumption of coronal ionization equilibrium is given in [32].

In the boundary of magnetically confined plasmas the highly radiating stages like Beryllium or Lithium like ions are transported to regions with electron temperatures which are considerably higher than those where these stages have the largest abundance in the coronal ionization equilibrium. Consequently, the effective cooling rate for all stages, $L_{eff} = P_{rad}/(n_e \sum_z n_z)$, is much higher in the plasma edge than expected for coronal equilibrium if transport is taken into account. This fact is illustrated in Fig. 13 where the effective cooling rates of neon in the case of coronal ionization equilibrium and of a transport dominated equilibrium are shown, the latter being typical for the discharges with a radiating boundary and improved energy confinement discussed in this report. Here, the radial distribution of impurity ions has been modelled with the transport code RITM [44] based on the coupled particle balance equations 72 and including radial impurity

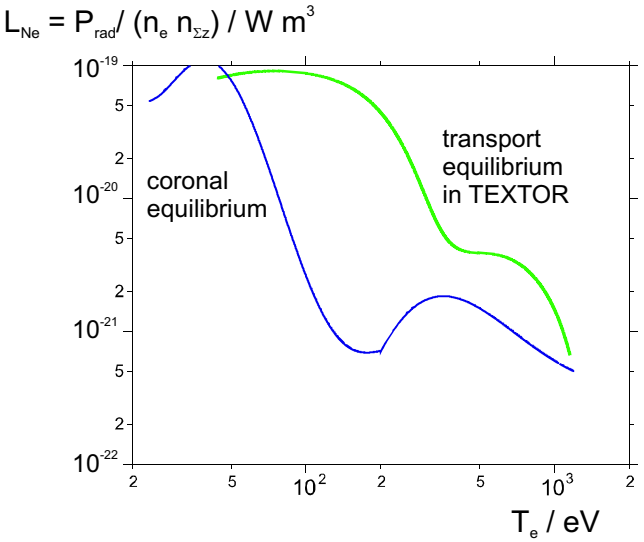

Figure 13: Effective cooling rate of neon in a coronal ionization equilibrium and in a transport dominated ionization equilibrium

flux densities according to Eqn. 74 with neoclassical and anomalous transport coefficients.

Beside the effective cooling rate a second global radiation characteristic has been proven useful to describe discharges with a radiating plasma boundary, the radiation potential E_{rad} [33]. The radiation potential describes the energy radiated by an impurity particle during its dwell time in the plasma. It is given by the ratio of the radiated power and the neutral influx as

$$E_{rad,Z} = \frac{P_{rad,Z}}{\Gamma_{0,Z}}. \qquad (75)$$

As a consequence, it is determined by the transport mechanisms of both the neutral particles which enter the plasma as discussed in section IV and the ions in their different ionization stages.

Finally, we want to illustrate the main features of the radiating plasma boundary in a simplified shell model [34], which allows us to relate the power radiated by impurities to the size of the toroidal confinement device, the major and minor plasma radius R and a, global discharge parameters as the line averaged central electron density $\bar{n}_e$ and the impurity concentration c_I, as well as transport parameters as the diffusion coefficient in the radiating layer $D_\perp$.

We start with the total radiated power density which is given by the sum of the radiated power densities from the ionization stages Z (Eqn. 70). If we integrate the radiated power density over the width of the radiating mantle at the boundary and assume that its extension is small with respect to the minor plasma radius, we can express the total radiated power loss P_{rad} as

$$P_{rad} = 4\pi^2 aR \sum_Z n_e^Z n_Z^Z L_Z(T_e^Z) d_Z. \qquad (76)$$

Here, n_e^Z and n_Z^Z are the characteristic densities of electrons and ions of ionization stage Z where the latter particles are mainly ionized, T_e^Z is the characteristic electron temperature and d_Z the characteristic width of their shell. Neglecting recombination and assuming diffusion as the dominant transport mechanism we can estimate d_Z as the distance along which the ions diffuse during their ionization time $\tau_{ion}^Z = (< \sigma v >_{ion}^Z (T_e^Z) n_e^Z)^{-1}$ as

$$d_Z = \sqrt{D_\perp^Z \tau_{ion}^Z} = \sqrt{\frac{D_\perp^Z}{< \sigma v >_{ion}^Z (T_e^Z) n_e^Z}}. \qquad (77)$$

Using a profile factor $f_{\rho,Z}$ which takes into account the change of particle densities over the radiating layer, we can express the total radiated power as a function of the global parameters $\bar{n}_e$ and c_I as

$$P_{rad} = 4\pi^2 aR \bar{n}_e^{3/2} c_I \cdot \sum_Z f_{\rho,Z} L_Z(T_e^Z) \sqrt{\frac{D_\perp^Z}{< \sigma v >_{ion}^Z (T_e^Z) n_e^Z}} \qquad (78)$$

It is important to note that the width of the individual shells is governed by both the ionization rate coefficient as a feature of the ionization stage under consideration and the transport characteristics which depend on the plasma scenario. Within the shell there are two processes occurring in parallel, the excitation of ions with the subsequent radiation and the ionization. Therefore, the hight of the radiated power density is determined by the number of photons released per ionization event which is given by the ratio of the respective rate coefficients for excitation leading to the most prominent radiative transitions like resonance transitions and for ionization. The larger the ionization energy with respect to the excitation energy the more photons are emitted per ionization event. This fact explains the strong reduction of the hight of the radiated power when we go from the beryllium and lithium- like states to the helium and hydrogen like states where excitation and ionization energy become more comparable. As a consequence, the radiated power density is considerably reduced once the lithium - like ions are ionized. This radial position marks the end of the radiating mantle towards the plasma center. As a rule of thumb, it is located where the local electron temperature amounts

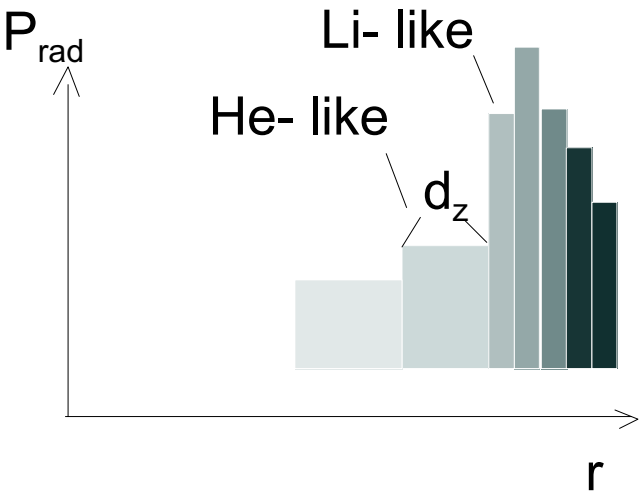

Figure 14: Shell structure of the radiating boundary layer

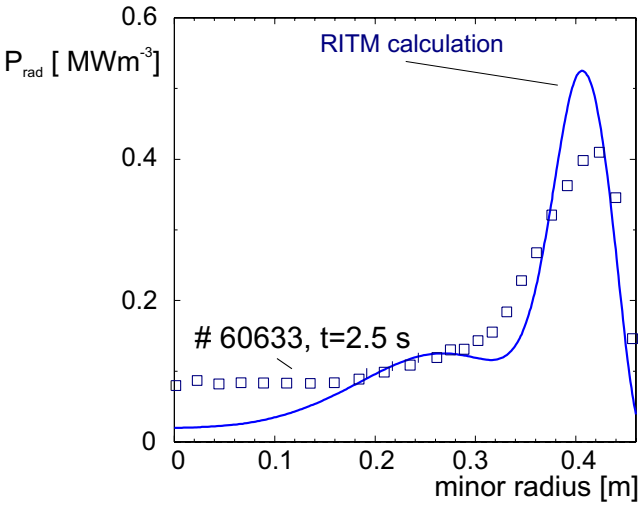

Figure 15: Radial profile of the radiated power density in a plasma with neon injection (squares) in comparison to a calculation with the transport code RITM.

to about a third to a half of the ionization potential of the lithium- like state.

With this we can estimate the extension of the radiating belt for various elements for a given temperature profile. However, one has to keep in mind that the temperature profile is strongly influenced by the radiation and the relation between temperature and radiation profile is therefore non- linear. Fig. 14 illustrates the qualitative features of the shell model with respect to the shell thickness and the hight of the radiated power density.

We end this section with an example of the radiated power density in a discharge in the TEXTOR tokamak, where 80 % of the total input power of 2 MW had been exhausted by neon radiation from the plasma edge (fig. 15). A comparison with the radiation profile calculated with the RITM code shows a good correspondence to the experimental data from bolometry.

Radiation from externally injected impurities will possibly have a significant contribution to the power exhaust in a future fusion device, the choice of a proper species, which determines the spatial region of the plasma where the radiation takes place (in particular the share between divertor radiation and main chamber radiation), has to be made in context with the choice of the wall materials and the associated radiation from the intrinsic impurities. A certain degree of control of both extrinsic and intrinsic impurities is desired to optimize the operational range for fusion in presence of the impurities.

ACKNOWLEDGMENTS

I wish to thank Michael Lehnen for Figs. 6 and 7 and for the model to calculate the parallel heat flux in the TEXTOR SOL.

.

REFERENCES

1. U. Samm, "Plasma- Wall Interaction", these proceedings.
2. P.C. Stangeby, "The Plasma Boundary of Magnetic Fusion Devices", Plasma Physics Series, IoP Publishing Ltd, Bristol, UK (2000).
3. A.V. Nedospasov and M.Z. Tokar', "Wall plasma in tokamaks", in Reviews of plasma physics, B.B. Kadomtsev (ed.), Vol. 18, Consultants Bureau, New York (1993).
4. R. Schneider, "Plasma edge physics for tokamkas", Laborbericht IPP Garching, IPP 12/1, February 2001
5. C.S. Pitcher and P.C. Stangeby, Plasma Phys. Control. Fusion **39** (1997) 779-930.
6. K.H. Finken, "Stochastic Plasma Edges and Dynamic Ergodic Divertor", these proceedings.
7. R. König et al., Plasma Phys. Control. Fusion **44** (2002), 2365.
8. D. Reiter, "Recycling and transport of neutrals", these proceedings.
9. D. Reiter, G.H. Wolf and H. Kever, Nucl. Fusion **30** (10) 2141 (1990).
10. S.I. Braginskii, "Transport processes in a Plasma", in Reviews of Plasma Phyiscs, M. Leontovich (ed.), Consultants Bureau, New York (1965), 205.
11. R. Chodura, "Plasma flow in the Sheath and Presheath of a Scrape-off Layer", "Physics of Plasma-

Wall Interaction in Controlled Fusion Devices", ed D.E. Post and R. Behrisch, Plenum Press, New York (1986), p. 99.

12. H. Gerhauser and H.A. Claassen, J. Nucl. Mater. **176-177**, 721 (1990).
13. M. Baelmans, D. Reiter and R.R. Weynants, Contrib. Plasma Phys., **36** 117 (1996).
14. M. Lehnen, M. Brix, U. Samm, B. Schweer, B. Unterberg and the TEXTOR- team, Nucl. Fusion **43** 168. (2003).
15. M. Lehnen, M. Brix, H. Gerhauser, B. Schweer and R. Zagorski, J. Nucl. Mater. **290-293** (3) 663 (2001).
16. V. Philipps et al., Nucl. Fusion **33** (6), 953 (1993).
17. P. Franzen and E. Vietzke, J. Vac. Sci. Technol. **A12** 820 (1994).
18. A. Pospieszczyk et al., J. Nucl. Mater. **266-269** 138 (1999).
19. M.F.A. Harrison in "Applied Atomic Collision Physics", Vol.2, Academic Press 1984, Eds. C.F. Barmett and M.F.A. Harrison (1984).
20. J.D. Hey et al., Contrib. Plasma Phys. **36** 583 (1996).
21. A. Pospieszczyk and Ph. Mertens, J. Nucl. Mater. **266-269** 884 (1999).
22. D. Reiter, J. Nucl. Mater. **196-198** 80 (1992).
23. B. Lehnert, Nucl. Fusion **8** 173 (1968).
24. H.P. Summers and M. von Hellermann, "Atomic and molecular data exploitation for spectroscopic diagnostics of fusion plasmas", in "Atomic and plasma- material processes in controlled thermonuclear fusion", Edt. by R.K Janev and H.W. Darwin, Elsevier, Amsterdam (1993), 87., http://adas.phys.strath.ac.uk/
25. H.R. Griem, "Plasma Spectroscopy", Mc Graw-Hill Book Company, New York (1964)
26. H.P. Summers and R.W.P. McWhirter, J. Phys. B **12** (1979), 2387.
27. R.W.P. Mc Whirter and H.P. Summers, "Atomic Radiation from Low Density Plasma" in Applied Atomic Collision Physics, Vol. 2, ed. C.F. Barnett and M.F.A. Harrison, Academic Press, Orlando (1984).
28. P. Grigull et al, Plasma Phys. Control. Fusion **43** (2001), A175.
29. S.A. Self and H.N. Ewald, Phys. Fluids **9** (1966), 2486.
30. M.Z. Tokar', M. Kobayashi and Y. Feng, Phys. of Plasmas **11** 2004, 4610.
31. D.E. Post, J. Nucl. Mater **220-222** (1995), 143.
32. R.V. Jensen and D.E. Post, Atomic Data and Nuclear Data Tables, **20** 5 (1977).
33. U. Samm, "Radiation control in a limiter tokamak", KFA- Report Jül- 2378 (1990).
34. M.Z. Tokar', Nucl. Fusion **34** (1994), 853.
35. M.Z. Tokar', Contrib. Plasma Phys. **34** (2/3) (1994), 344.
36. A. Gibson and M.L. Watkins, Proc. of the 8th Europ. Conf. on Controlleld Fusion and Plasma Physics, Prague (1977), Vol. I, 31.
37. K. Lackner and J. Neuhauser, IAEA Technical Meeting on Divertors and Impurity Control, Garching (1981), 58.
38. U. Samm et al., Proc.of the 18th EPS. Conf. on Controlleld Fusion and Plasma Physics, Berlin (1991), ECA Vol. 15C, part III, 157.
39. U. Samm et al., Plasma Phys. Control. Fusion **35** (1993), B167.
40. U. Samm et al., J. Nucl. Mater. **220-222** (1995), 25.
41. U. Samm et al., J. Nucl. Mater. **196-198** (1992), 633.
42. U. Samm, M.Z. Tokar' and B. Unterberg, J. Nucl. Mater. **241-43** (1997), 827.
43. A.M. Messiaen et al., Phys. Rev. Lettr. **77** (1996), 2487.
44. M.Z. Tokar', Plasma Phys. Control. Fusion **36** (1994), 1819.